Angewandte Chemie
Eine Zeitschrift der Gesellschaft Deutscher Chemiker

Supporting Information

69451 Weinheim, Germany

Three-Dimensional Chemical Patterns for Cellular Self-Organization**

*Yevgeniy V. Kalinin, Jatinder S. Randhawa, and David H. Gracias**

anie_201007107_sm_miscellaneous_information.pdf
anie_201007107_sm_suppvideo1.mov

Supplementary figures and text

Note 1	Generation of spatial patterns in two dimensions.
Figure S1	Two-dimensional linear gradients.
Note 2	Temporal control: Details of conceptual estimate.
Figure S2	Temporal control numerical simulation results.
Note 3	Methods to speed up loading of the containers.
Figure S3	SEM images of containers with pore size reduced by gold electrodeposition.
Video S1 Caption	Movie of image sequences (19 images total) showing self-organization of *E. coli* into a helix over a period of 25 min.

Supplementary Note 1. Generation of spatial patterns in two dimensions.

We note that our methodology can be utilized to generate both 2D and 3D spatial chemical patterns. The 3D patterns are described in the main text; here, we describe the generation of 2D linear gradients. These gradients were formed by utilizing parallelepiped-shaped containers with porous slits along their long axis. Numerical simulations suggested that it was necessary to create an exponentially shaped and asymmetrically positioned slit (closer to one edge than the other, **Figure S1a**) to generate a linear gradient at a distance in the range of approximately 100 μm outside the container (**Figure S1c**). Hence, we utilized such a pattern with minor variations in this design such as breaking up the continuous slit into four discrete pores to increase mechanical strength (**Figure S1b**).

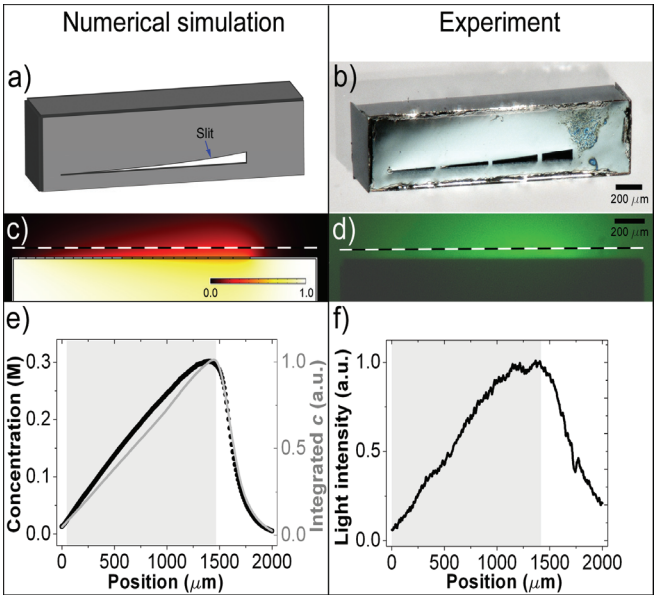

Figure S1. Two-dimensional linear gradients. a) Schematic diagram of the pore slit pattern derived from numerical simulations that is required to generate a linear gradient using a parallelepiped shaped container. b) Optical image of the self-assembled container. c) Numerically simulated, and d) fluorescence image of experimentally realized gradients of fluorescein released from these containers. e) Quantitative numerical simulation result along the dashed line (in panel c) showing the formation of a linear gradient pattern of fluorescein. The thick solid line (in panel e) represents concentration values at the points that lie in the plane of the slit on the dashed line (panel c) itself while the thin line (in panel e) shows the integrated concentration in the plane parallel to the side of the container and containing the dashed line (panel c). f) Corresponding experimentally realized gradient along the dahsed line in panel d) showing good agreement with simulations.

After fabrication, the containers were positioned in a stationary gel and we observed that fluorescein was released from these containers in a linear gradient (**Figure S1d**) with excellent quantitative agreement between numerical simulations (**Figure S1e**) and experiments (**Figure S1f**). Use of this polyhedral container shape for linear gradient

generation also readily facilitates control over the steepness of the gradient by scaling the dimensions of the slit.

Supplementary Note 2. Temporal control: Details of conceptual estimate.

A simple analytical model can be used to validate our numerical simulations. An order of magnitude estimate can be used to gain insight behind the underlying concept of chemical release (in stationary media) from a porous membrane in a spherical geometry[33,34] (**Figure 1a** of the main text). We can assume that the rate-limiting step for chemical release is diffusion through the side wall and that the initial concentration outside the container is zero; this assumption works well for small pore sizes. It follows from Fick's law[34] that the rate of chemical release through the pores can be written as

$$V\frac{dc}{dt} = -D\frac{c}{w}A \qquad \text{(Eq. 1)}$$

Here D is the diffusion coefficient, c is the chemical concentration (assumed uniform within the container), V is the container volume, w is the container wall thickness (equal to the pore length for straight pores), A is the total area of the pores and t is the time.

Solutions of Eq. 1 have the form,

$$t = -\frac{\pi}{6}\frac{d^3 w}{DA}\ln\{\frac{c}{c_0}\}, \qquad \text{(Eq. 2)}$$

where c_0 is the initial concentration inside the container and d is the container diameter. Hence, we can estimate the characteristic time scale for release $\tau = \frac{\pi}{6}\frac{d^3 w}{DA}$ discussed in the main text. This estimate suggests that larger containers (100 μm on the side and larger) and sufficiently small pores (~100 nm and smaller) can extend the duration of chemical release to days, months and even years.

Numerical simulations shown in Figure 5a of the main text agree with these conceptual estimates. Additionally, numerical simulations show that the rise and fall of the released chemical at a fixed spatial point away from the container can be engineered by varying the pore size (**Figure S2a**). As a consequence, chemical release can be achieved with a concentration variation of 10% over specified time duration; this time is plotted in **Figure 5a** of the main text.

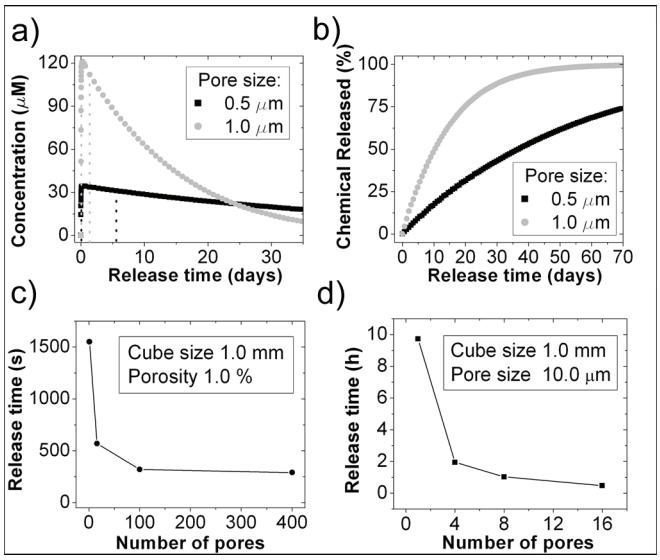

Figure S2. Temporal control numerical simulation results a-b) Temporal variation of, a) concentration at the specific time point at a fixed spatial point a distance *d* from the center, and b) total integrated concentration inside the container, both for a *d* = 1.0 mm sized container for two different pore sizes. The curves shown are typical but the slopes decrease for larger containers and smaller pores. c-d) Temporal variation of chemical release from a cubic container plotted against the number of pores, while maintaining, c) the same porosity, and d) the same pore size. Both curves were generated assuming a square pore distribution with uniform spacing and centrosymmetry.

A plot of the total chemical released as a function of time (**Figure S2b**) suggests that there is no initial burst that is often observed in polymer dissolution based controlled release systems.[19, 20] The temporal release characteristics are also affected by the pore distribution (**Figure S2c-d**). For the same porosity, a smaller pore size (and consequently larger numbers of uniformly spread out pores) results in shorter release times from containers (**Figure S2c**). With equally sized pores, an increase in porosity also results in shorter release times (**Figure S2d**).

Supplementary Note 2 References

[33] E.L. Cussler, *Diffusion: Mass Transfer in Fluid Systems*. (Cambridge University Press, 1997).
[34] J. Crank, *The Mathematics of Diffusion*. (Clarendon Press, Oxford, 1956).

Supplementary Note 3. Methods to speed up loading of the containers.

One concern with our methodology is that containers that release chemicals over long periods of time would also take a long time to load. We note that in these applications, loading can be sped up by one of the following methods.

a) Increasing external loading concentration: Regarding diffusion based loading in stationary media, the most effective way to speed up loading of chemicals into the containers is to increase the concentration of the chemical in the medium outside of the container. Increasing the concentration outside increases the chemical flux directed into the container in direct proportion to the concentration difference as governed by Fick's law. For example, we estimate that the loading time for a 1 mm cubic container with 1.0 μm pores, 1×10^{-4} % porosity, similar to the one shown in **Figure S3a** with 1×10^{-6} M of fluorescein would decrease from over 1 month to less than a week when the concentration of the chemical into which the container was placed (for diffusion based loading) was increased from 2×10^{-6} M to 1×10^{-4} M. We note that practical solubilities of various chemicals [For example, the solubility of fluorescein in water is approximately 10^{-4} M while that of uranine (sodium salt of fluorescein) is several orders of magnitude larger] will ultimately determine the maximum concentration of the chemical into which the chemical can be immersed, and hence the minimum loading times.

b) Stirring the medium during loading: We note that increasing mass transport by heating or mechanical stirring would also increase loading rates.

c) Finally, it is also possible to build containers with one completely open face so that chemicals can be rapidly introduced into the container. Elsewhere, such a technique was utilized to load the containers with mammalian cells for insulin delivery. [29] One drawback of this approach is that a

separate sealing step is required after loading and additionally it would be challenging to engineer porosity on this sealed face of the polyhedron.

These and other loading methods continue to be explored in our laboratory.

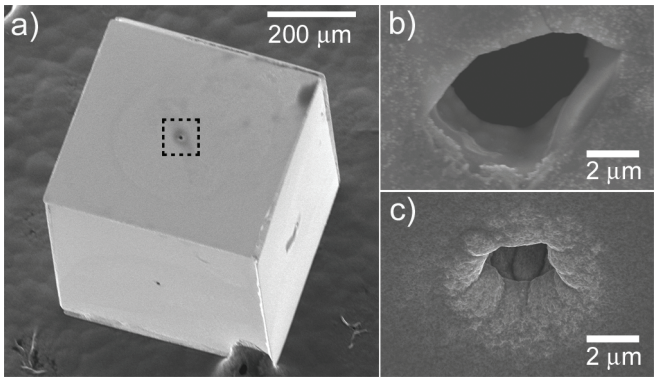

Figure S3. Temporal control over pattern generation by varying pore size. a) Scanning electron microscope (SEM) image of a container (d = 500 μm) with a single pore in the center. Zoomed-in SEM images of a single pore with the exterior diameter of b) 10 μm and c) 2 μm, formed after gold plating.

Supplementary Video S1 Caption. Movie of image sequences (19 images total) showing self-organization of *E. coli* into a helix over a period of 25 min. The time interval between sequences is approximately 1-2 min.